ON THE IUE POINT SPREAD FUNCTION AT LOW RESOLUTION*

A. Cassatella, J. Barbero, P. Benvenuti

1. INTRODUCTION

In this paper we intend to review the spectral and spatial resolution performances obtainable with IUE low resolution spectra complementing the sparse information already available with new data to clarify aspects not sufficiently studied before.

Previous work shows that the instrumental resolution (both spatial and spectral) of IUE low dispersion spectra is primarily dependent on the focussing conditions in the telescope and on the wavelength (de Boer, Koornneef and Meade, 1980; Ponz and Cassatella 1981; Barbero and Cassatella 1982 and 1983; Panek, 1982).

The focussing conditions in the telescope are assumed to be well represented by the focus STEP, which is a linear function of three temperatures at different heights of the telescope so providing a measure of its thermal dilatations. The STEP values are recorded in the Log scripts accompanying each image obtained.

The first problem we studied is the repeatability of the resolution performances (here parameterized through the FWHM of the spectra both perpendicular and parallel to the dispersion direction) at a given STEP and wavelength. This will allow the detection of any dependence of the resolution properties on other observing parameters. Such a study, done in Section 2, indicates that, at a given wavelength, the low resolution point spread function (PSF) depends only on focus STEP, although second order dependence on other parameters cannot be excluded.

The next aspect we studied is the dependence of the full width at half maximum (FWHM) perpendicular to the dispersion on the telescope focus at given wavelengths in order to determine the range of STEP in which the focussing conditions are optimum (Section 3).

A number of images of continuous sources obtained at optimum focus were then selected for each operational camera (LWR, LWP and SWP) in order to determine the dependence of the FWHM perpendicular to the orders on wavelength for both large and small aperture spectra (Section 4).

*Reprinted from IUE ESA Newsletter No. 18, December 1983, pp. 38-69.

In section 5 we examined the behaviour of the spectral resolution as a function of wavelength using a large number of low resolution spectra of emission line objects. The analysis was restricted to the LWR and SWP camera because not enough data were available for the LWP. The results in Section 4 and 5 were then compared to deduce information on the two-dimensional shape of the low resolution PSF (Section 6).

The asymmetries of the PSF perpendicular to the dispersion are studied in Section 7 and a comparison is made with analytical profiles.

Finally, to help in the analysis of spectra of extended sources, a study is provided in Section 8 of the PSF perpendicular to the dispersion based on several spectra of point sources trailed at constant rate in a direction approximately parallel to the major axis of the large apertures.

It is important to note that the data analysed in this paper, except those presented in Section 7, were obtained through the IUE low resolution standard processing (IUESIPS) installed at VILSPA on 10 March 1981 and at GSFC on 4 November 1980.

In particular, the line by line spectra were used to study spatial resolution, while the extracted spectra were used to study the spectral resolution. This ensures that IUE users can easily reproduce our results and make comparisons.

As far as the units are concerned, we generally used the pixel as unit for the widths of the profiles perpendicular to the dispersion (1 pix corresponds to 1.51± 0.04 arcsec on the sky; Panek, 1982), although the quantity directly measured from the line by line spectra is the diagonal pixel ($\sqrt{2}$ pix). The spectral resolution was measured in Å, but was also reported in pixels in the figures of Section 5. The conversion between wavelength units along the dispersion and pixels can be easily done using the dispersion constants (Panek, 1983). Indicating with ΔZ the distance in pixels along the dispersion direction we have:

$\Delta\lambda/\Delta Z =$ 1.669 Å/pix for the SWP
2.646 Å/pix for the LWP
2.652 Å/pix for the LWR

2. REPEATABILITY OF RESOLUTION PERFORMANCES

Previous studies concord in that the resolution (spectral and spatial) depends on the focussing conditions in the telescope and on wavelength. However, while on the one hand these dependences were not definitively determined before, on the other some suspicious discrepancies with respect to the expectations were occasionally reported. Therefore we want first to clarify to what degree of accuracy the two-parameter dependence is adequate. For this purpose, we selected 5 LWP images of point sources obtained with focus step exactly equal to -1.4, and measured the FWHM perpendicular to the dispersion in 7 wavelength bands 200 Å wide centered at λ = 1900, 2100, 2300, 2500, 2700, 2900 and 3100 Å. Measurements derived from spectral regions found to be over-exposed were rejected. The relevant information on images used is contained in Table 1.

In each of the wavelength bands the r.m.s. deviation of the FWHM about the mean is 0.06 to 0.07 pixels, corresponding to a relative error of 2 to 3% on the FWHM. The individual measurements for all the images and the mean values are reported in Figure 1 as a function of wavelength. Note that the images used for this test were obtained with values of the camera head amplifier temperature (THDA) over a rather wide range. However, no correlation is apparent, at the same wavelength, between the FWHM and the THDA. The same result is reported by de Boer et al. (1980) for the SWP and LWR cameras.

The above repeatability test was also extended to the SWP and LWR cameras. Although only few images were available for these cameras with exactly the same focus STEP, the results show that the repeatability is the same as for the LWP. A further confirmation of the degree of repeatability is given in Section 3.

We conclude therefore that the spatial resolution properties are adequately parametrized through the focus STEP and the wavelength. Occasional deviations are probably due to incorrect recording of the STEP values in the observation scripts.

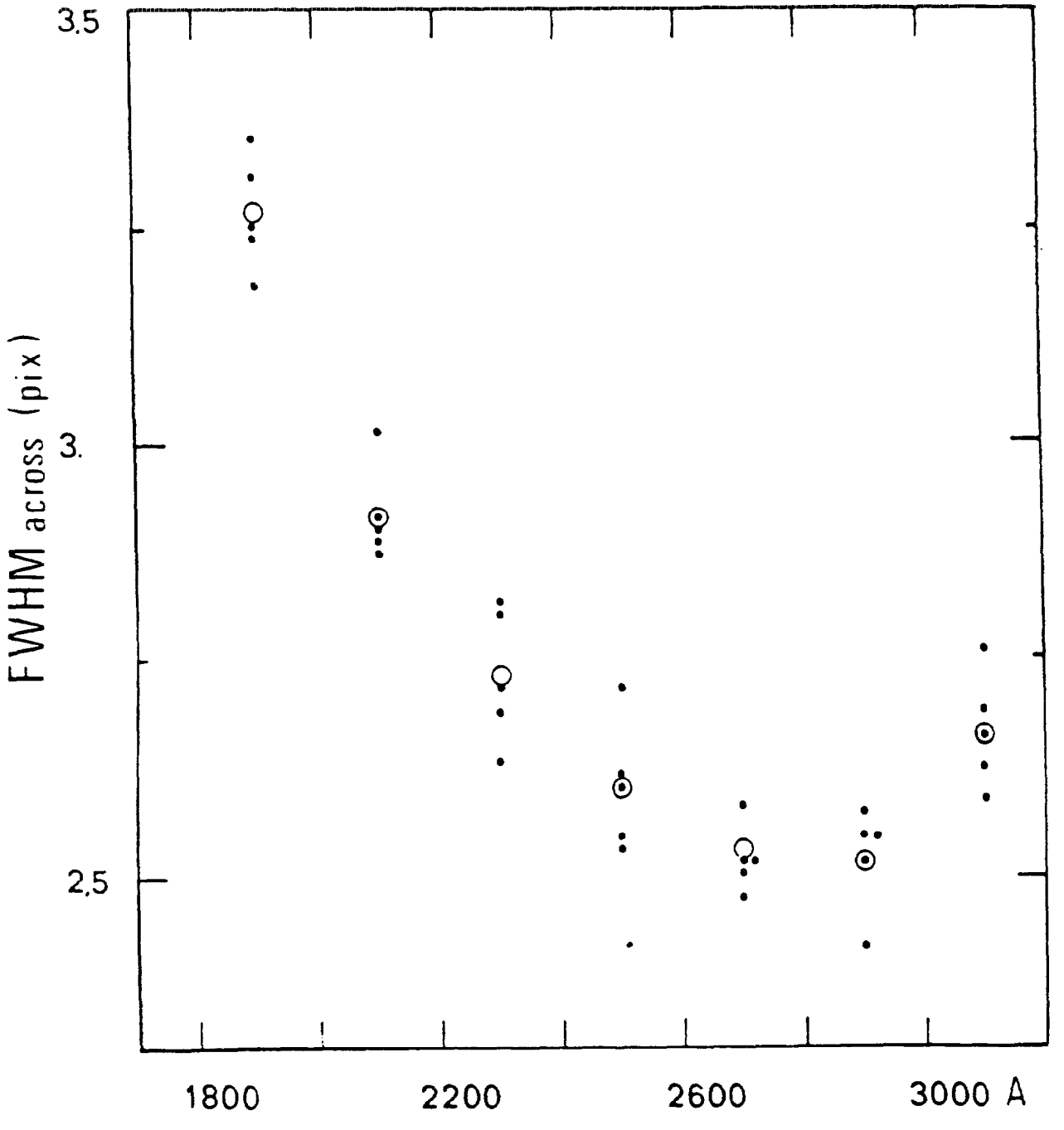

FIGURE 1

Repeatability test of the telescope focussing conditions at the same focus STEP using cross profiles of LWP spectra. The FWHM of the cross profiles appears to be repeatable to within 2 or 3%. Open dots represent the mean of the individual measurements.

-TABLE 1-

IMAGE	TARGET	THDA (K)	EXP. TIME (sec)
LWP 1326	BD + 75° 325	7.8	10
LWP 1801	HD 60753	10.5	6
LWP 1447	BD + 28° 4211	12.5	100
LWP 1448	BD + 28° 4211	12.8	75
LWP 1529	BD + 28° 4211	8.5	52

3. OPTIMUM FOCUSSING CONDITIONS

The focussing conditions in the IUE telescope are currently assumed to be optimum for STEP values close to -1. In order to verify this point we used several SWP, LWR and LWP images of point sources (generally IUE calibration standards) obtained through the large apertures and with a wide range of focus STEP. These data were used to study how the FWHM across the dispersion varies as a function of STEP in given wavelength bands (1350±50 Å and 1850±50 Å for the SWP; 2100±75 Å and 2700±75 Å for the LWP; 2700±75 Å for the LWR). Note that, as shown in Section 5 and 6, the PSF along the dispersion is less sensitive to variation of STEP than is the PSF across the dispersion. Our measurements span the range in STEP from about -3.7 to 3.5 for the SWP, -3.3 to 0.5 for the LWR and -2.0 to 1.5 for the LWP.

The results are shown in Figure 2a,b,c for the SWP, LWP and LWR, respectively.

The figures allow us to distinguish between two separate ranges of focus STEP:

- a plateau extending from STEP $\simeq$ -1 to more negative values, in which the FWHM takes the minimum values. The mean values of the FWHM in the plateaux and the corresponding r.m.s. deviations are reported in Table 2.

- a linear region in which the FWHM increases with STEP. This region extends from STEP $\sim$ 0 in the SWP and STEP $\sim$ -1 in the LWP and LWR, to more positive values. A linear regression analysis of

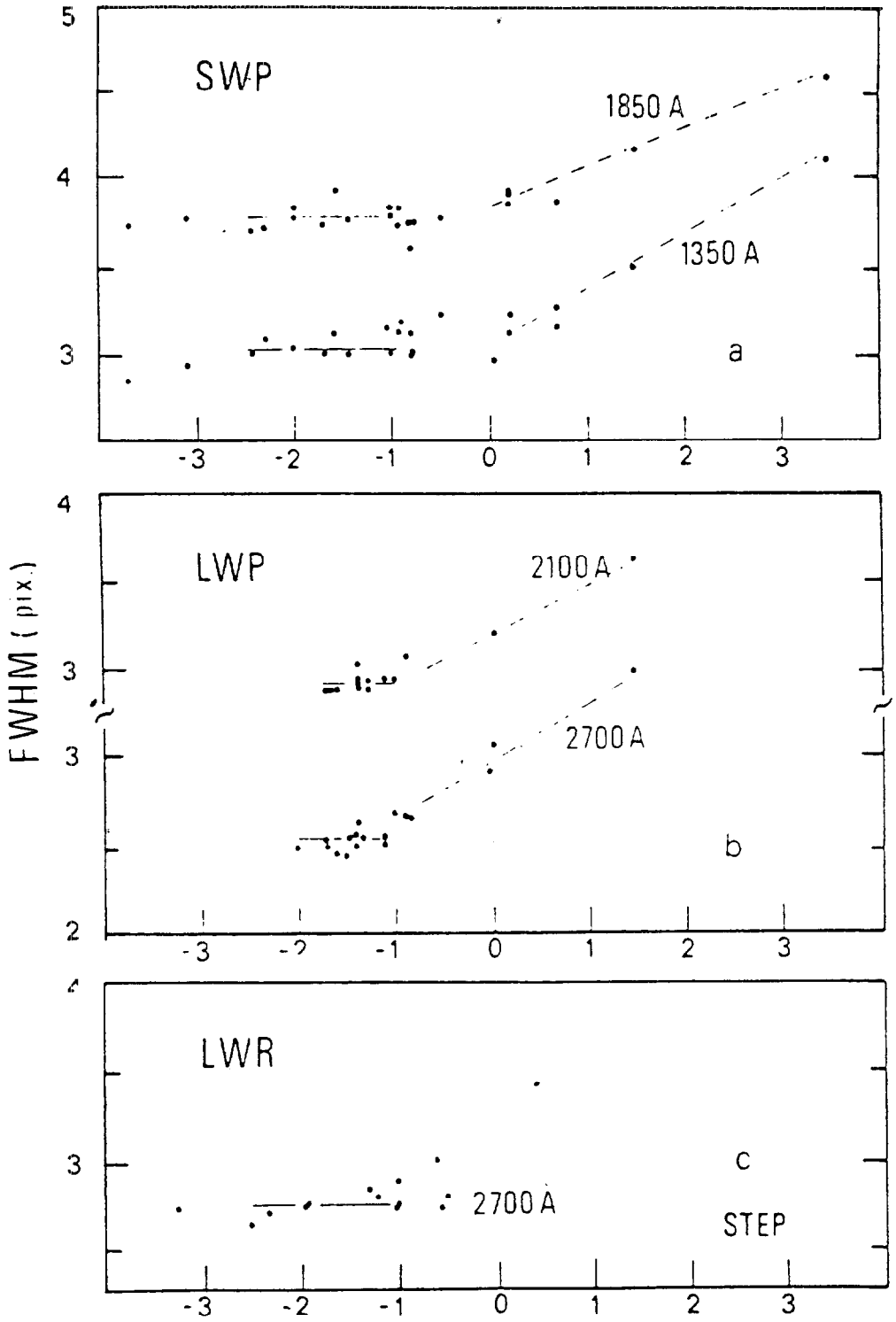

FIGURE 2

Test of the optimum focussing conditions in the IUE telescope. The figure shows the behaviour of the FWHM perpendicular to the dispersion as a function of focus STEP for the SWP, LWP and LWR cameras (curves a, b and c respectively). The measurements refer to the indicated wavelength bands. The plateau region (FWHM const) defines the optimum range of focus STEP.

the data in this region indicates that the slope ΔFWHM/ STEP is nearly the same for both SWP and LWP as indicated in Table 2. Similar information is not available for the LWR since no data with well documented, positive STEP values, were found in the archive.

-TABLE 2-

a) Plateau:

CAMERA	STEP RANGE	AVERAGE FWHM (pix)
SWP	-2.5 To -1.0	3.06 ± 0.06 (1350 Å)
		3.80 0.07 (1850 Å)
LWP	-2.0 To -1.0	2.90 0.04 (2100 Å)
		2.52 0.09 (2700 Å)
LWR	-2.5 To -1.0	2.74 0.09 (2700 Å)

B) Linear region:

CAMERA	STEP RANGE	ΔFWHM/ΔSTEP
SWP	0.0 To 3.5	0.23 (1350 Å)
		0.33 (1850 Å)
LWP	-1.0 To +1.5	0.28 (2100 Å)
		0.35 (2700 Å)

Some important conclusions can be drawn from this analysis:

- at any wavelength it is possible to define a range of STEP values at which optimum focussing conditions are produced. This range can be safely limited as $-2 \leq STEP \leq -1$ (plateau region), irrespective of camera used.

- the repeatability of FWHM across the orders is very good in the plateau regions (2-3%) confirming the results of Section 2.

We finally note that a statistical analysis on all images taken at VILSPA during the months of November 82 and May 83 indicates that the average STEP value was -1.3 ± 0.6. Therefore, since IUE observations are, on average, done at optimum focussing conditions, it makes sense to construct average curves (FWHM across and parallel to the dispersion v.s. wavelength) at optimum focussing conditions as they are representative of many practical cases. Such curves will be presented in Section 4.

4. SPATIAL RESOLUTION AS A FUNCTION OF WAVELENGTH

Information on the spatial resolution attainable from low dispersion spectra in the direction perpendicular to the dispersion can be obtained from the width of the cross profiles as a function of wavelength.

Previous work by de Boer et al. (1980), Ponz and Cassatella (1980), Panek (1982) and Barbero and Cassatella (1982 and 1983) indicates that the width of the cross profiles is wavelength dependent and shows a minimum around 1400 Å in the SWP spectra, while it is a decreasing function of lambda in the LWR and LWP spectra, at least for $\lambda \leq 2900$ Å.

The published curves FWHM v.s. wavelength, although similar in shape, show however a non-negligeable scatter one with respect to the other. In order to construct new average curves representative of optimum focussing conditions (see Section 3), we then made a very accurate selection of images of well exposed low resolution spectra observed through both large and small apertures. We stress that only images with well documented and appropriate focus STEP were included. The STEP values considered, in order to ensure the representativity of optimum focussing conditions, all lie within or close to the plateau regions defined in Section 3.

Note that the exposure times were very short for the images used in this analysis: this guarantees that no appreciable changes of focus STEP have occurred during the exposures.

The cross profiles were extracted from the line by line spectra in bands 150 A wide in the SWP and 200 Å wide in the LWP and LWR. Special bands 40 Å wide centered at 1240 Å, 1350 Å and 1550 Å were also considered for the SWP camera in order to exclude the Lyα region, (first band), to include the region where the FWHM is minimum (second band) and to exclude a reseau mark at 1585 Å in the small aperture spectra (third band). Reseau marks present in the

long wavelength cameras were avoided as well.

The average curves FWHM across the orders v.s. wavelength are presented in Figures 3 a, b and c for the SWP, LWP and LWR cameras respectively. Error bars (r.m.s.) are also indicated. The curves are the result of averaging 7 images for the SWP, 10 images for the LWP and 5 images for the LWR. The images used are listed in Table 3. The data in Figure 3 are also reported in Table 4 for convenience.

It is important to note that spectral regions found to be underexposed or overexposed in some of the images were not used. The overall shape of the curves in Figure 3 agree very well with the latest average curves reported (Barbero and Cassatella, 1983).

Because of the better selection of the images used, the larger amount of data, and the careful verification of the STEP values, the above curves are believed to represent suitably the optimum focussing conditions (close, as shown in Section 3 to the average observing conditions).

It is interesting to note that the curves FWHM v.s. wavelength show a pronounced minimum in the SWP camera around 1350 Å, while the minimum FWHM is reached toward the end of the spectral range (~2900 Å) for both LWP and LWR.

A first glance to Figure 3 shows that the width of the spectra is about the same, on average, for small and large aperture SWP spectra. This is not true for the long wavelength cameras where the small aperture spectra appear to be systematically broader than large aperture spectra. By averaging the individual measurements, it is actually possible to see that the ratio between the FWHM perpendicular to the dispersion in the large relative to small aperture spectra is 1.0± 0.02 for the SWP, and 0.96± 0.02 for both the long wavelength cameras.

Figure 3 shows also that both long wavelength cameras provide, on average, a better spatial resolution than the SWP camera. This is particularily true for the LWP camera which is also better than the LWR by about 9% (averaged over wavelength in the large aperture).

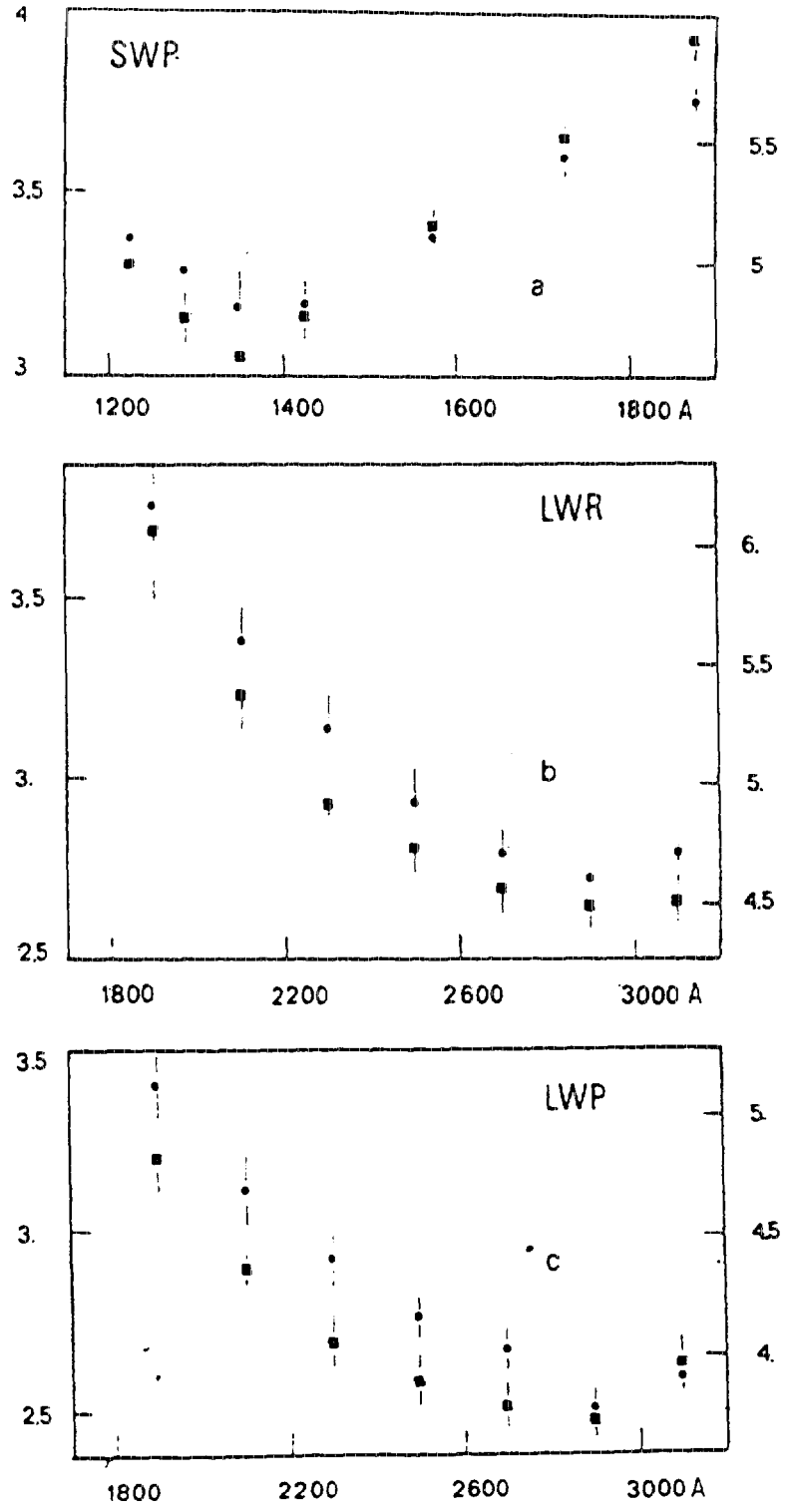

FIGURE 3

FWHM perpendicular to the dispersion as a function of wavelength for the SWP, LWR and LWR cameras (curves a, b and c, respectively). The FWHM values are reported both in pixels and in arcsec. Squares and dots represent large and small aperture data, respectively. Error bars (r.m.s.) are indicated.

-TABLE 3-

Images used for the study of the FWHM
across the orders v.s. wavelength

IMAGE	STEP	EXP.TIME (sec) SAP	LAP	TARGET
SWP 13475	-1.0	28	14	BD+75°325
SWP 16388	-0.91	6	3	HD 93521
SWP 18065	-0.93	28	14	BD+28°4211
SWP 18067	-1.70	52	26	BD+28°4211
SWP 18881	-1.44	78	26	BD+28°4211
SWP 19124	-2.45	300	85	HD 111786
SWP 19594	-0.79	9	3	HD 93521
LWP 1676	-1.70	40	20	BD+75°325
LWP 1326	-1.40		10	BD+75°325
LWP 1254	-1.10	40	20	BD+75°325
LWP 1788	-1.73	9	3	HD 93521
LWP 1501	-1.60	4	2	HD 93521
LWP 1251	-1.1	60	50	BD+28°4211
LWP 1529	-1.4	180	52	BD+28°4211
LWP 1447	-1.4		100	BD+28°4211
LWP 1448	-1.4		75	BD+28°4211
LWP 1801	-1.38	18	6	HD 60753
LWR 8553	-2.5	120	60	BD+28°4211
LWR 14233	-1.9	48	24	BD+75°325
LWR 15625	-1.3	570	190	BD+33°2642
LWR 10129	-1.0	48	24	BD+75°325
LWR 12061	-1.2	6	3	HD 93521

-TABLE 4-

FWHM perpendicular to the dispersion (in pixels)
as a function of wavelength

λ(Å)	LARGE APERTURE FWHM	r.m.s.	SMALL APERTURE FWHM	r.m.s.
SWP				
1125	3.65	± 0.21	3.58	± 0.20
1240	3.30	0.04	3.32	0.11
1275	3.15	0.08	3.28	0.13
1350	3.05	0.06	3.18	0.11
1425	3.15	0.07	3.20	0.07
1575-1550*	3.41	0.06	3.38	0.03
1725	3.65	0.04	3.59	0.06
1875	3.93	0.06	3.75	0.04
LWP				
1900	3.23	± 0.11	3.41	± 0.13
2100	2.90	0.08	3.11	0.11
2300	2.70	0.08	2.91	0.08
2500	2.59	0.08	2.76	0.07
2700	2.52	0.07	2.67	0.06
2900	2.47	0.07	2.50	0.04
3100	2.63	0.08	2.59	0.04
LWR				
1900	3.69	± 0.20	3.76	± 0.13
2100	3.24	0.10	3.38	0.10
2300	2.93	0.11	3.14	0.10
2500	2.81	0.08	2.93	0.10
2700	2.70	0.08	2.79	0.07
2900	2.65	0.07	2.73	0.03
3100	2.66	0.07	2.80	0.03

* the band at 1575 Å refers to large aperture spectra

-TABLE 5-

GEOMETRIC CORRECTION RESIDUALS

Central position of the spectrum in the line-by-line spectra (diagonal pixels)

CAMERA	SWP		LWP			LWR	
λ(Å)	LARGE	SMALL	λ(Å)	LARGE	SMALL	LARGE	SMALL
1275	27.96	28.06	1900	28.32	28.28	27.78	27.74
1425	27.94	28.11	2100	28.12	28.29	27.77	27.67
1575	28.18	28.07	2300	28.03	28.04	28.00	27.99
1725	28.22	28.16	2500	27.99	28.02	28.00	27.93
1875	28.12	28.03	2700	27.87	27.81	28.09	28.03
			2900	28.00	27.07	28.15	28.05
			3100	28.12	28.18	28.20	28.10

Note that in the case of two sources falling into the large entrance aperture of the spectrographs, these can be resolved provided their distance perpendicular to the dispersion direction is:

$$d \gtrsim 0.849\ \mathrm{FWHM}$$

(c.f. with equation 1 in Section 5). Since the minimum value of the FWHM perpendicular to the dispersion is (at optimum focussing conditions) about 4.6 arcsec and 4.0 arcsec for the SWP and LWR, respectively, this implies for example that large aperture double spectra can be separated provided their distance is larger than ~3.9 or ~3.4 arcsec respectively. This is demonstrated in Figure 4 where we show two cross profiles double spectra in the SWP (around 1600 Å) obtained exposing the target twice (with the same exposure time) in two different points distant 3.9 and 6.1 arcsec along the major axis of the large aperture: in the latter case the two profiles are separated while they are not resolved in the former case.

For the analysis of large aperture spectra of extended sources it is sometimes important to disentangle the

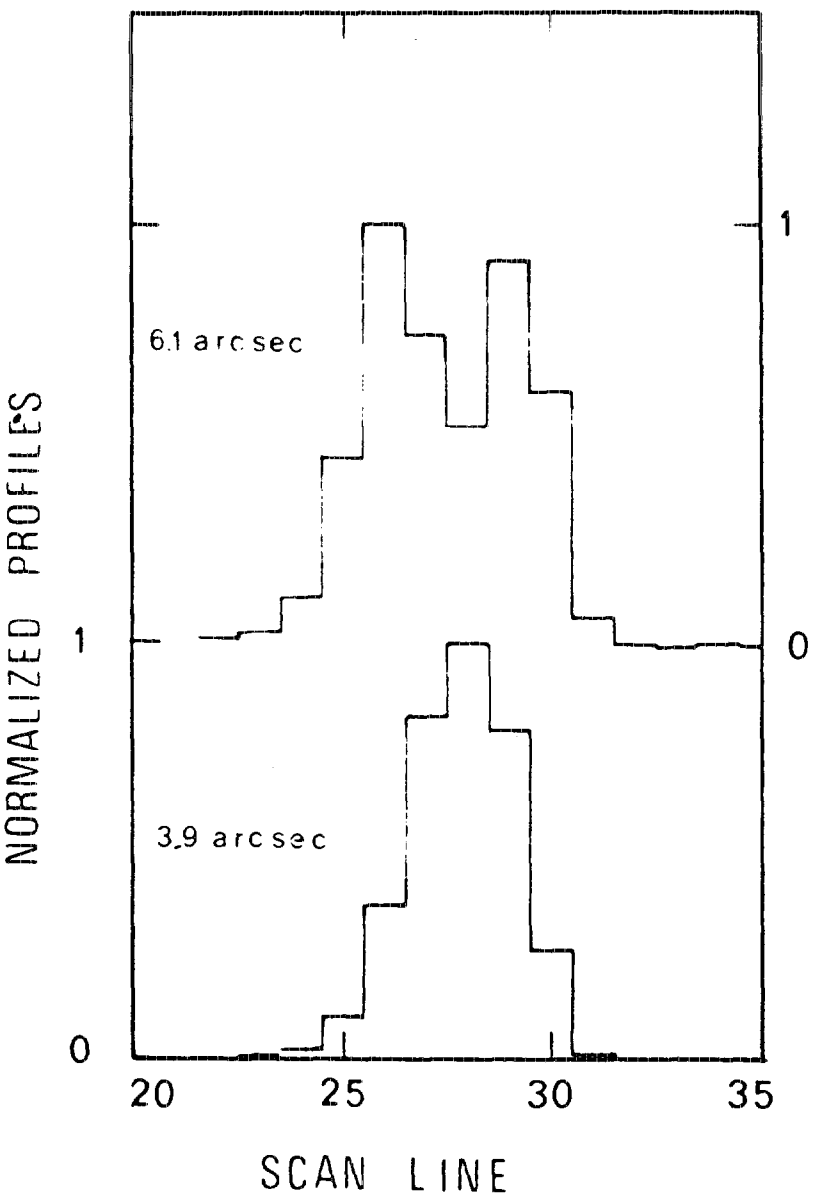

FIGURE 4

Cross profiles of two double spectra around 1600 A. The spectra were obtained by exposing the target twice in two different points of the large aperture distant 3.9 (bottom) and 6.1 arcsec along the major axis of aperture. Abscissae represent the scan line number (in diagonal pixels) oriented towards the large aperture.

residual geometrical distorsions in the direction perpendicular to the dispersion from spatial inhomogeneities intrinsic in the source. In order to determine the geometrical correction residuals, we selected well exposed images of calibration standards taken through both large and small apertures (12, 13 and 10 images for the SWP, LWP and LWR, respectively). The line-by-line spectra were averaged in bands 150 Å or 200 Å wide for the SWP and the LWP and LWR cameras respectively. A gaussian profile was then fitted to the average cross profiles and the central position of the spectrum X_c (which is scan line 28 in principle) was determined. The values X_c v.s. wavelength for both large and small aperture spectra are reported in Table 5 for the three cameras. The data are also shown in Figure 5. The typical r.m.s. error on the mean X_c is 0.10 pixels, irrespective of wavelength and camera used. Figure 7 indicates that the geometric correction residuals (X_c-28) for both small and large aperture spectra are very similar within the same camera. As expected, the residuals are negligeable near the center of the cameras. These statistical results are in good agreement with those of Panek (1982). No evident correlation has been found between the geometric correction residuals and THDA or focus STEP.

5. SPECTRAL RESOLUTION

Information on the spectral resolution at low dispersion may be found in Boggess et al. (1978), Cassatella and Penston (1978), Clavel (1980) and Ponz and Cassatella (1981). However, the wavelength dependence of the resolution was not considered in detail.

In order to provide an extended set of direct measurements of the spectral resolution we used about 20 SWP and 10 LWR low resolution spectra of emission line sources (RR Tel, V 1016 Cyg, AG Dra, Z And, CI Cyg, Mira Ceti B) and measured about 80 emission lines in the SWP and 40 in the LWR.

The measurements were done by fitting a gaussian profile to the emission lines in the extracted spectra as provided by IUESIPS. A major source of inaccuracy was the location of the continuum, especially at longer wavelengths, where the crowding of the emission lines is often important. This makes the results rather uncertain for the LWR camera.

In this analysis we also made use of images with STEP values outside the optimum focussing range (see Section 3). This is not expected to change the validity of the results

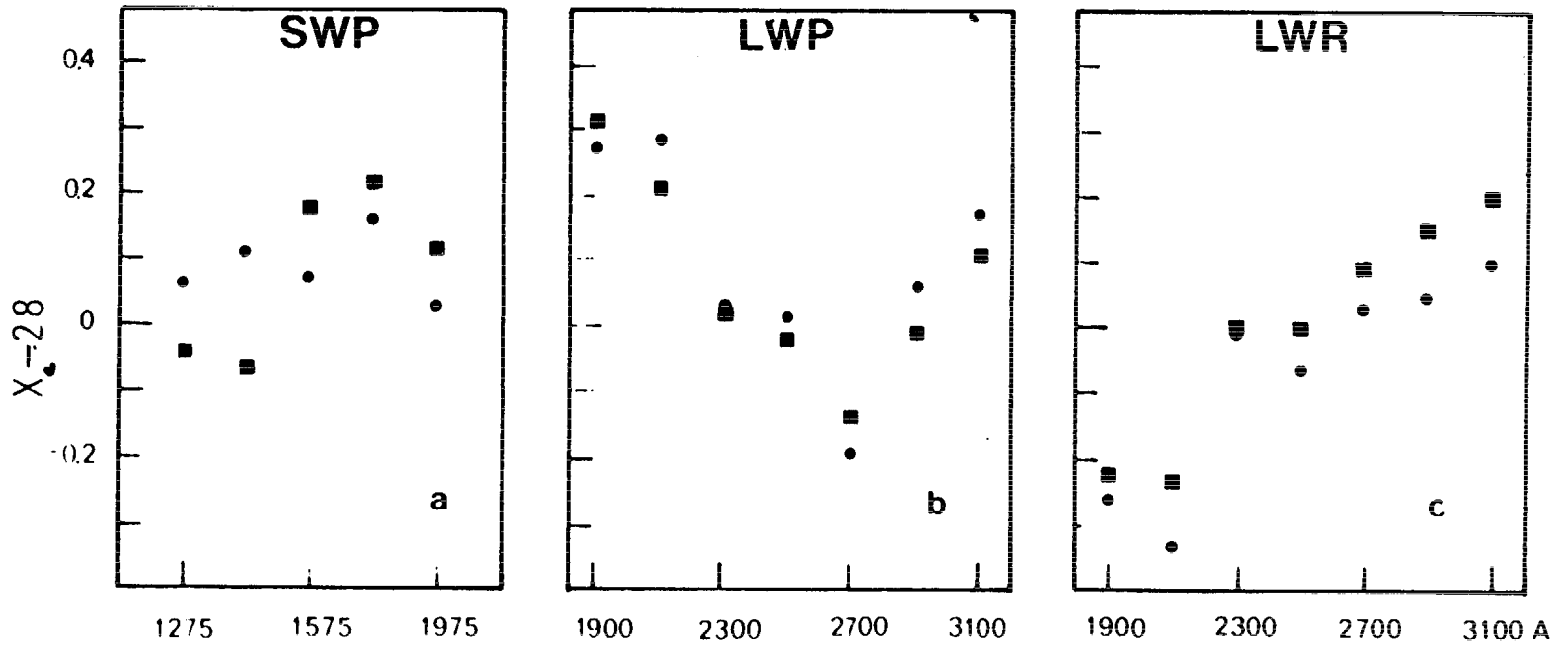

FIGURE 5

Geometric correction residuals X_c-28 (diagonal pixel) for the SWP, LWP and LWR cameras (curves a, b, and c respectively) as a function of wavelength.

since, as shown later in this section, the spectral resolution (along the dispersion) is sensibly less dependent on the focussing conditions than is the spatial resolution (perpendicular to the dispersion).

The relevant results of the gaussian fitting, i.e. the FWHM (in Å) of the emission lines along the dispersion direction are shown in Figure 6 and 7 for the SWP and LWR cameras, respectively. The agreement with the previous results by Barbero and Cassatella (1983) is good for the SWP camera while large discrepancies exist for the LWR camera in the region from 2400 to 2800 Å. This discrepancy is mainly due to the use, in the previous report, of emission lines of poor quality, which were rejected in this analysis. Note also that the behaviour of FWHM v.s. lambda is rather uncertain at the short wavelength end of the SWP camera ($\lambda \lesssim 1300$ Å). Actually, the only lines usable are OVI 1218 Å and NV 1240. The former is generally faint and not completely reliable, while the latter is a doublet.

Figures 6 and 7 show that the best resolution is obtained around 1400 Å in the SWP camera and around 2400 Å in the LWR camera. This compares well with the blaze wavelengths of the short and long wavelength spherical gratings, i.e. 1400 Å and 2500 Å, respectively.

The actual resolution can be easily evaluated from the curves FWHM v.s. wavelength in Figures 6 and 7 using:

$$\Delta\lambda = 0.5\sqrt{2/\ln 2}\ \ \mathrm{FWHM} = 0.849\ \mathrm{FWHM} \qquad (1)$$

which represents the minimum wavelength separation necessary for two gaussian lines of width FWHM and equal central intensity to be resolved i.e. to show a minimum half way between their central wavelengths. The above equation implies for example, that in agreement with what is observed, the SiIV and MgII doublets (around 1400 Å and 2800 Å respectively) can be at least partially resolved with IUE low resolution spectra. An interesting result which can be derived from Figures 6 and 7 is the possible gain in resolution using small aperture spectra relative to large aperture spectra. The observations actually indicate that such a gain exists for SWP images, of the order of 8% on average, while the gain is very little (~3%) and probably not significant for the LWR spectra.

No reliable information about the spectral resolution could be derived for the LWP camera, essentially because of the lack of data on emission line sources. The existing data seem to indicate, however, that the spectral

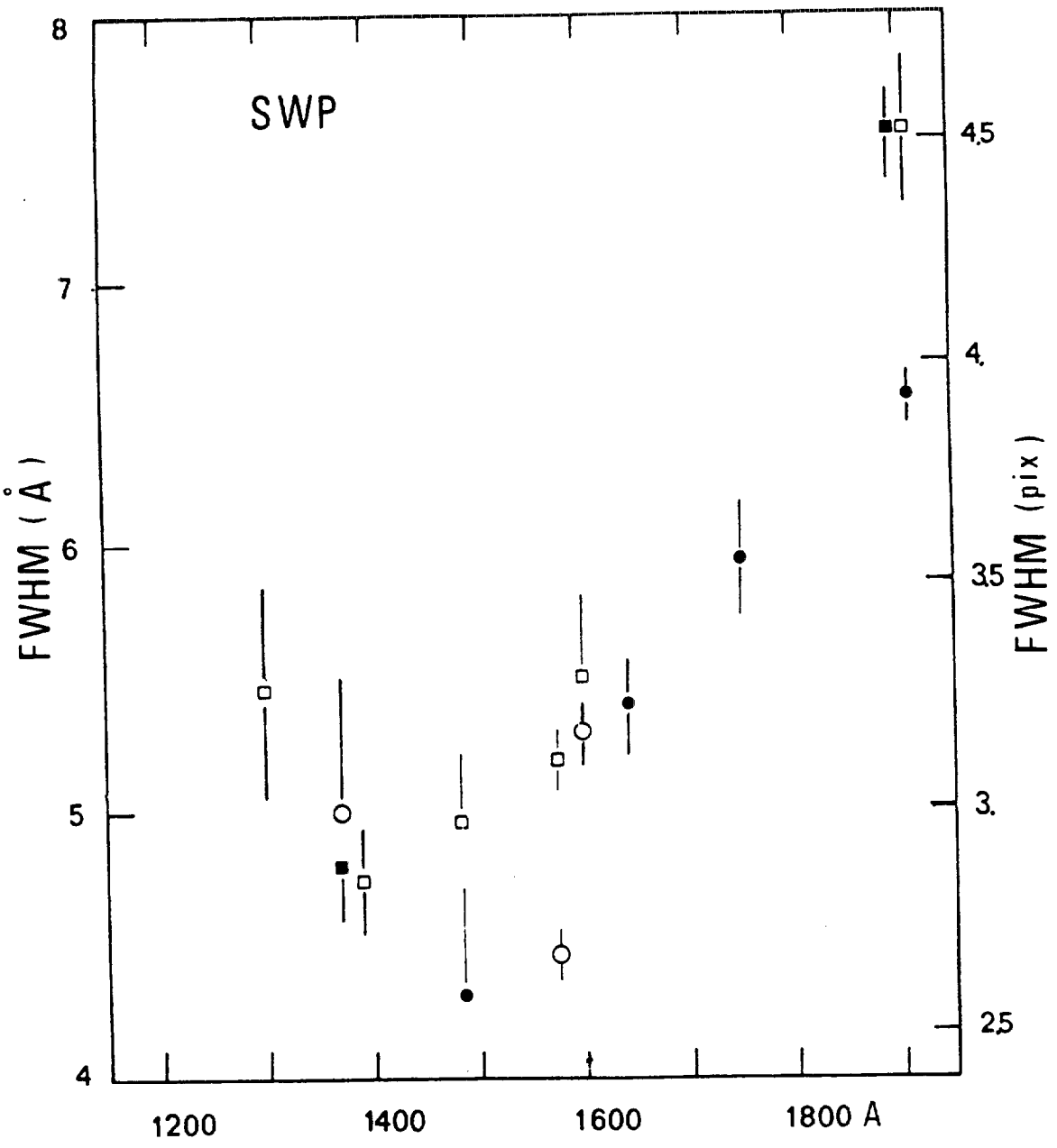

FIGURE 6

FWHM along the dispersion as a function of wavelength for the SWP camera obtained from spectra of emission line objects. Squares and dots represent data from the large and small aperture respectively. Open and filled symbols represent data obtained from 2 to 3 measurements or 4 to 8 measurements respectively.

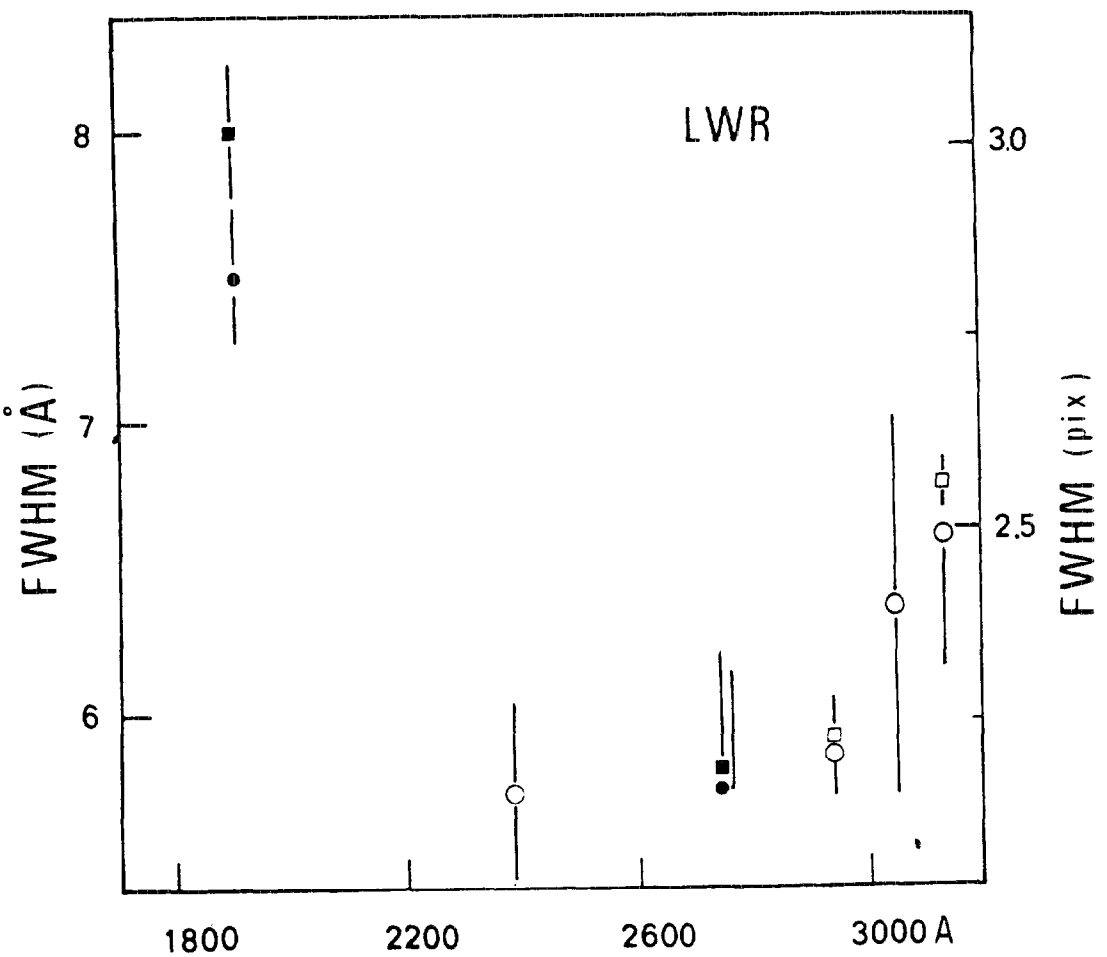

FIGURE 7

Same as Figure 6 for the LWR camera.

resolution performances of the LWP are $\lesssim$ 10% better than for the LWR. Similar results have been reported by Imhoff (1983) who finds that high resolution LWP images of the on-board Ne-Pt wavelength calibration lamps provide a better resolution than LWR images of the same kind, in most of the spectral range covered by the cameras. Note that, as discussed in Section 4, the spatial resolution of the LWP is also on average 9% better than the LWR.

We finally want to comment about the dependence of the spectral resolution on focussing conditions. Test images of RR Tel taken on March 31, 1980 at three different focus steps from -2.1 to 3.3 indicate that the spectral resolution is not significantly sensitive to the variation of STEP, while the contrary is true for the widths of the profiles perpendicular to the dispersion. This assures us that the results presented in this section are representative of the average observing conditions.

6. TWO-DIMENSIONAL SHAPE OF THE POINT SPREAD FUNCTION

A first look to low resolution images of emission line sources indicates immediately that the emission lines have a different two-dimensional shape according to the position in the image. This is seen as for example, in Figure 8 which shows amplified sections of three low resolution large aperture images of RR Tel corresponding to three different spectral regions: the short wavelength end (lines of OVI 1218 Å and of NV 1240 Å), the central region (NIV] 1486 Å), and the long wavelength end of the camera (SiIII] 1893, CIII] 1909 Å). One image (SWP 8610) was taken at good focussing conditions (STEP = -2.1), while the other two, (SWP 8607 and SWP 8606) had a bad focus (STEP = 1.4 and 3.3, respectively).

It is apparent from Figure 8 that the emission lines are roughly symmetric near the camera center while they appear elongated in the dispersion direction towards the long and the short wavelength ends of the camera.

Also, it is possible to verify, as concluded at the end of the previous section, that the width of the emission lines in the dispersion direction is about the same in the well focussed image as in the badly focussed images, while the profiles perpendicular to the dispersion are clearly broader in the latter ones. This confirms that changes of focus STEP mainly affect the spatial resolution rather than the spectral resolution.

The two-dimensional shape of the low resolution PSF can be deduced from Figures 9a and b where we report, as a

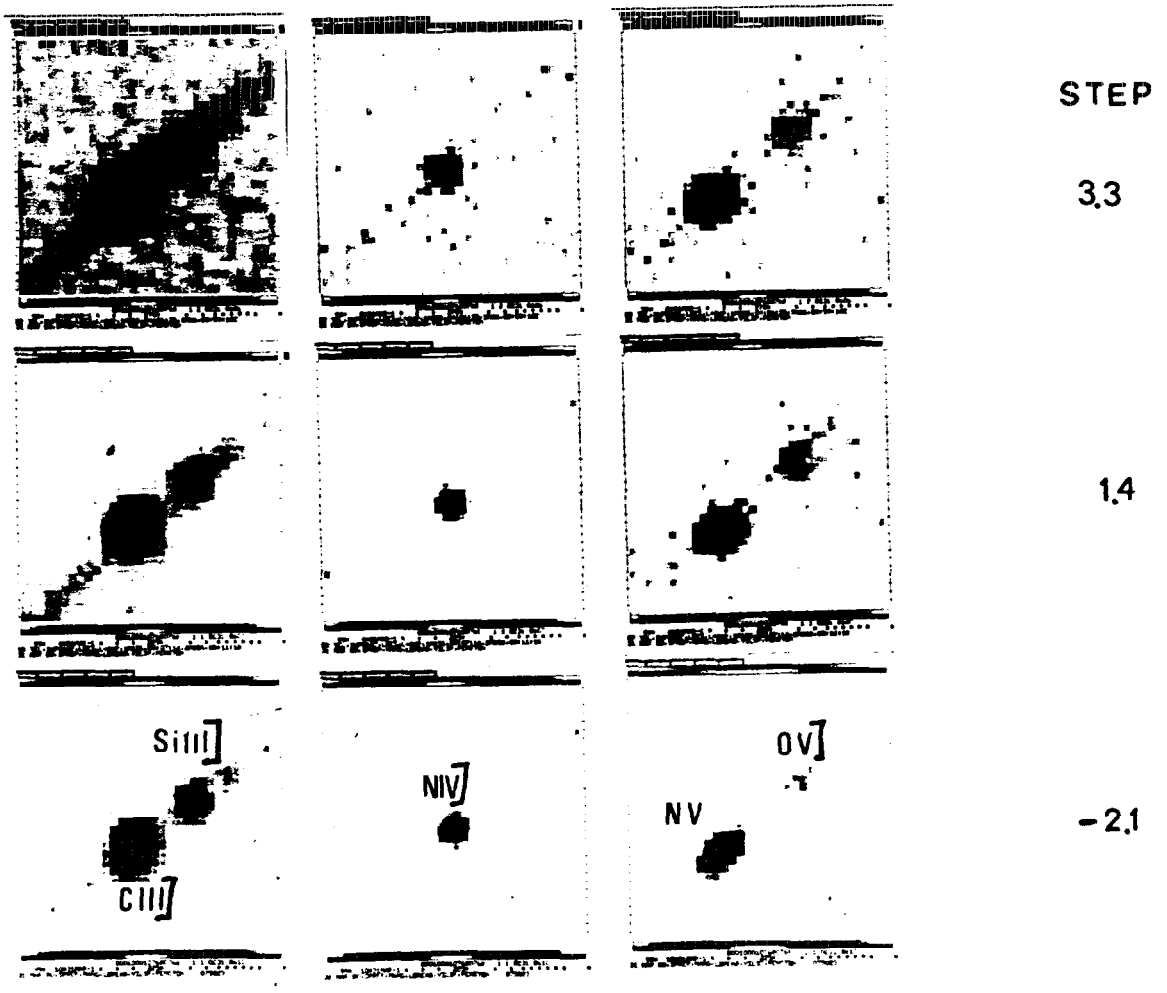

FIGURE 8

From top to bottom: three sections of SWP 8606, 8607 and 8610. From right to left: the CIII] 1909 and Si II] 1893 Å lines, the NIV] 1486 Å line, and the NV 1240 and OVI 1218 Å lines. The focus STEP is very bad for SWP 8606 (3.3), is bad for SWP 8607 (1.4) and good for SWP 8610 (-2.1).

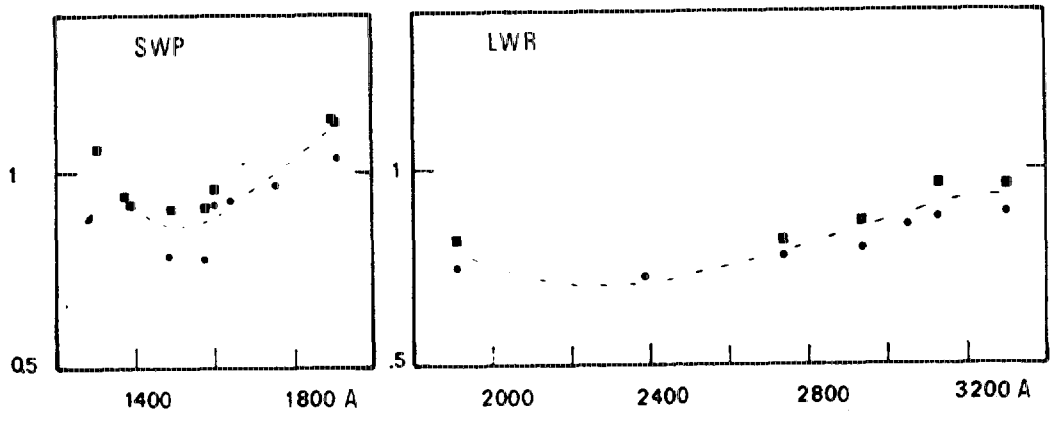

FIGURE 9

Ratio between the FWHM along and across the dispersion for the large (squares) and small (dots) aperture spectra as a function of wavelength in the SWP and LWR cameras.

function of wavelength, the ratio of the FWHM along the dispersion to the FWHM across the dispersion for both SWP and LWR cameras. The values of FWHM were obtained from the data in Figures 3a and c (FWHM across the dispersion) and 6 and 7 (FWHM along the dispersion), interpolating the first set of curves corresponding to the data in Figure 6 and 7. Figure 9 clearly confirms the results of the visual inspection of Figure 8, as described above. Figure 9 also indicates that the ratio FWHM(along)/FWHM(across) depends strongly on wavelength for the SWP, contrary to the LWR, case. For the SWP camera we have on average:

$$\text{FWHM(along)/FWHM(across)} = \begin{cases} 1.06 \pm 0.16 & \text{large aperture} \\ 0.94 \pm 0.13 & \text{small aperture} \end{cases}$$

while for the LWR camera we find:

$$\text{FWHM(along)/FWHM(across)} = \begin{cases} 0.87 \pm 0.07 & \text{large aperture} \\ 0.81 \pm 0.06 & \text{small aperture} \end{cases}$$

These results compare very well with those of Ponz and Cassatella (1981) derived from the analysis of spectra of RR Tel.

7. ANALYTICAL SHAPE OF THE PSF PERPENDICULAR TO THE DISPERSION

The profiles along the dispersion direction, as derived from the extracted spectra of emission line sources, do not indicate any detectable asymmetry, and can suitably be represented by gaussian profiles. The same is found in high resolution spectra (Fricke, 1983). This is not the case for the cross profiles which generally show evident asymmetries (at least for the SWP). An accurate knowledge of the analytical profile across the dispersion is clearly important as in the case of two partially resolved sources falling in the large entrance aperture and the astronomer wanting to extract separately the two spectra by fitting the cross profiles with analytical functions. To this purpose, we analysed a few selected line-by-line spectra obtained at optimum focussing conditions, namely SWP 18881 and SWP 18067 of BD + 28° 4211, LWR 10129 of BD + 75° 325 and LWP 1676 of BD + 75° 321. In order to get a better resolution on the cross

profiles, we used a special modification of the IUESIPS which provides a sampling interval of half diagonal pixel in the direction perpendicular to the dispersion, instead of one diagonal pixel as in the standard software.

The line-by-line spectra were averaged in bands 50 A or 200 Å wide for the SWP and the LWP and LWR, respectively. The average cross profiles were then fitted through a χ^2 fitting algorithm which makes use of either the following analytical functions:

a) a gaussian profile represented by:

$$y = y_o \exp\left\{ - \ln 2 \left[\frac{2(x-x_o)}{FWHM} \right]^2 \right\} \qquad (2)$$

where y_o and x_o are the peak intensity and the central position, respectively. The area beneath this curve is:

$$A = \frac{1}{2} \left[\frac{\pi}{\ln 2} \right]^{1/2} y_o \; FWHM \qquad (3)$$

b) a skewed function represented by:

$$y = y_o \exp\left\{ -\ln 2 \left[\frac{\ln[1+2b(x-x_o)/f]}{b} \right]^2 \right\} \qquad (4)$$

for $2b(x-x_o)/f > -1$,
and $y = 0$ for $2b(x-x_o)/f \leq -1$.

Changing the value of b, a different degree of skewness is obtained. As $b \rightarrow 0$ eq. 4 reduces to a symmetrical gaussian function. The parameter f is related to the full width at half maximum as follows:

$$f = \frac{FWHM \times b}{\sinh b} \qquad (5)$$

while the area beneath curve (4) is:

$$A = \frac{1}{2}\left[\frac{\pi}{\ln 2}\right]^{1/2} y_o \; f \; \exp\left[\frac{b^2}{4\ln 2}\right] \qquad (6)$$

The results of this analysis can be summarized as follows:

1) The r.m.s. deviation of observed with respect to fitted analytical profiles is very good in all cases, irrespective of camera used and analytical shape adopted, ranging typically from 0.2×10^{-4} to 3×10^{-4}

2) The skewed function is decidely a better representation for the SWP profiles as indicated by the very small σ-values approaching 1.2×10^{-4}, compared with sigmas a factor about 7-10 larger for the gaussian representation. On the contrary, for the LWP and LWR the fitting accuracy is about the same with either the representations, eq. 2 or eq. 4. This is due to the fact that the short wavelength spectra do show an asymmetry, while the long wavelength spectra are only marginally asymmetric. This is clearly seen in Figure 10 where a comparison is shown between observed and analytical profiles for the image SWP 18881 (large aperture data) around 1425 Å.

A closer analysis of the values of b obtained after the fitting points towards the same conclusion: b (which measures the degree of asymmetry) is larger for the SWP, while it is closer to zero for the two long wavelength cameras. The way b varies with wavelength is shown in Figure 11 for the two SWP large aperture spectra 18067 and 18881. It is interesting to note that the behaviour of b v.s. wavelength is very similar for the two images confirming that b actually describes an optical property of the spectrograph. Note that the value of b is smaller for the SWP small aperture spectra analysed here than for the large aperture spectra, becoming of the same order only at longer wavelengths.

3) A comparison of the areas beneath the fitted curves indicates that, for the SWP, about 1.3% more flux is extracted using the skew function than with the gaussian function. Since the former representation has been shown to be best for the SWP we conclude that the flux is more accurate too.

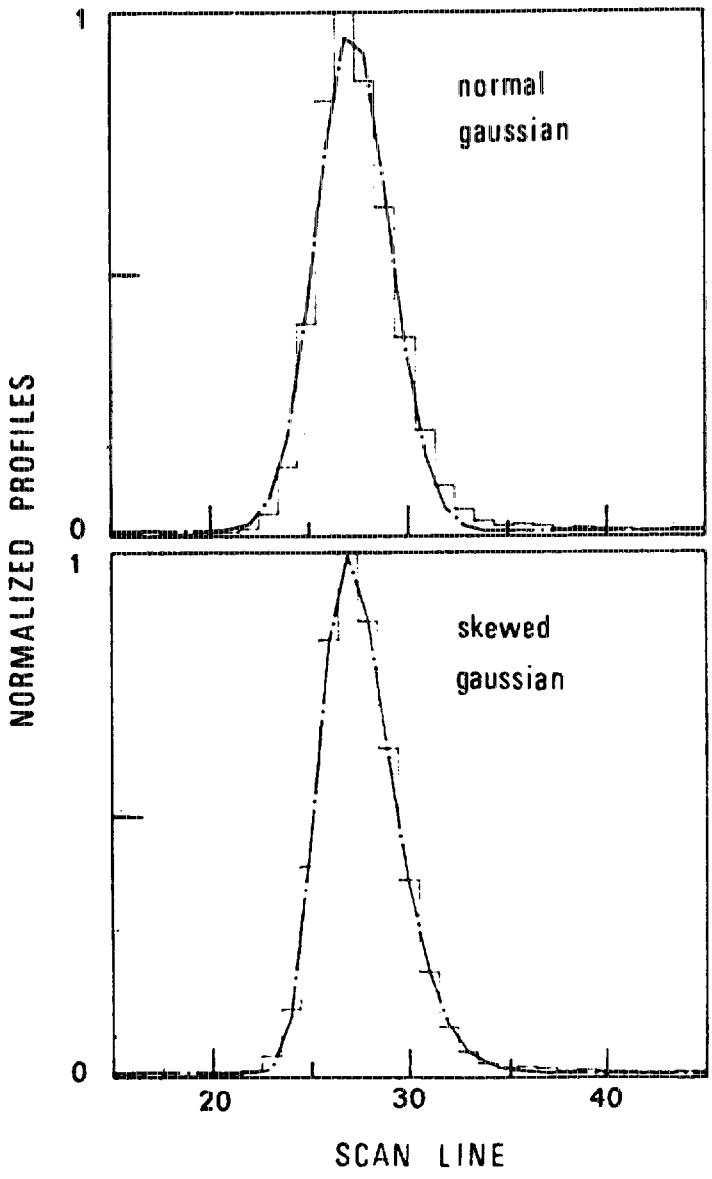

FIGURE 10

Comparison between observed profiles perpendicular to the dispersion and analytical profiles around 1425 Å. Top: comparison with a normal gaussian profile (eq. 2) bottom: comparison with a skewed gaussian (eq. 4). Abscissae are in units of $\sqrt{2}/2$ pixels counted from the large to the small aperture.

8. CROSS PROFILES OF EXTENDED SOURCES

In order to help in the analysis of extended source spectra observed at low resolution, we studied the instrumental profile of the large apertures in the direction perpendicular to the dispersion using trailed spectra of IUE calibration standards. The trailing procedure is performed by maneuvering the IUE spacecraft in such a way the star crosses both edges of the large aperture from positive to negative X_{FES} coordinates of the Fine Error Sensor (FES) while keeping the Y_{FES} approximately constant and equal to the Y coordinate of the centre of the large apertures.

Since the large apertures of both the short and long wavelength spectrographs each have a small inclination with respect to the direction Y_{FES} = constant (about 13° counted clock wise from the major axis of the apertures to the negative X_{FES} axis), the cross profiles of trailed spectra are taken to represent suitably the response of the large aperture when observing homogeneous extended sources. The results are presented in Figures 12 a, b and c for the SWP, LWP and LWR, respectively. The profiles were obtained by averaging the profiles of 6 to 8 trailed spectra for each camera.

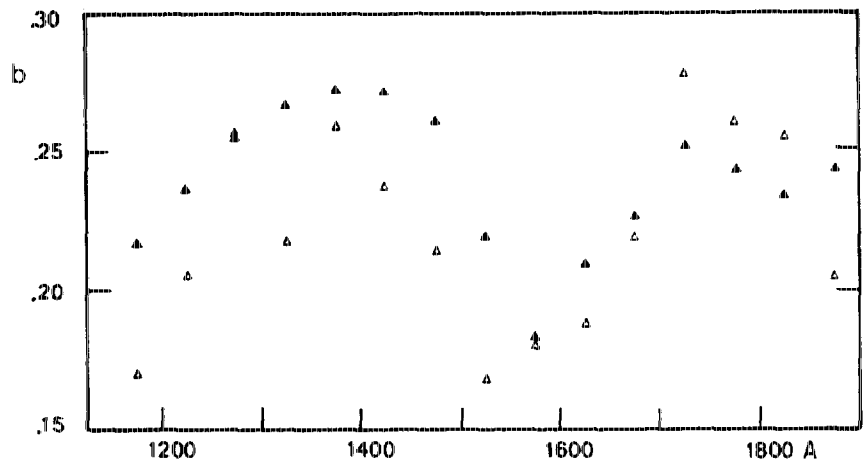

FIGURE 11

Variation of the skew parameter b (eq. 4) as a function of wavelength for SWP 18067 (open triangles) and SWP 18881 (filled triangles). The data refer to large aperture spectra.

FIGURE 12 (Overleaf)

Normalized cross profiles obtained from averaging trailed spectra of IUE standard stars obtained with the SWP (a), LWP (b) and LWR (c) cameras. Abscissae are in diagonal pixels counted from the small to the large aperture for the SWP and LWR and from the large aperture to the small aperture for the LWP.

NORMALIZED CROSS PROFILES

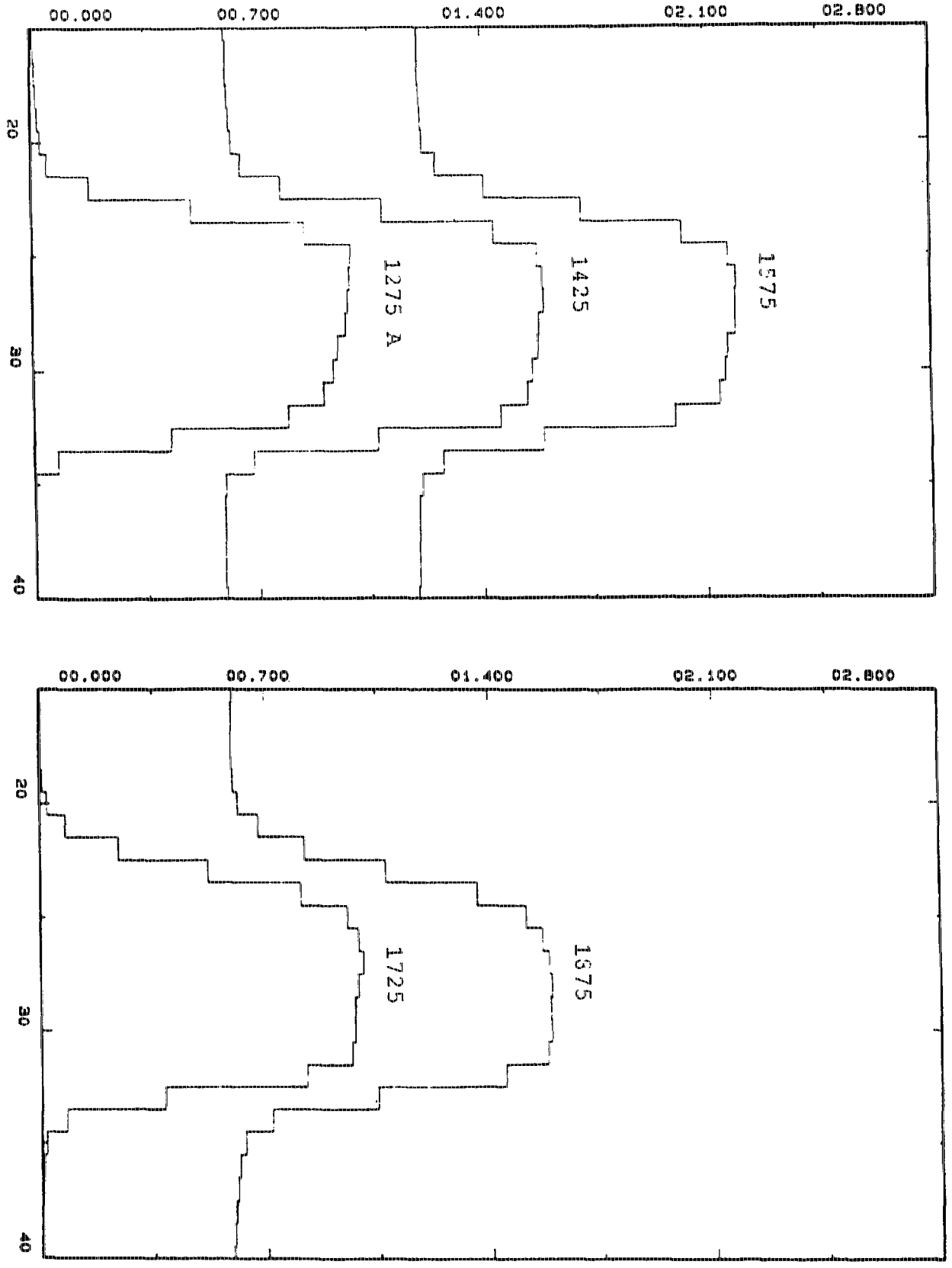

- FIGURE 12a -

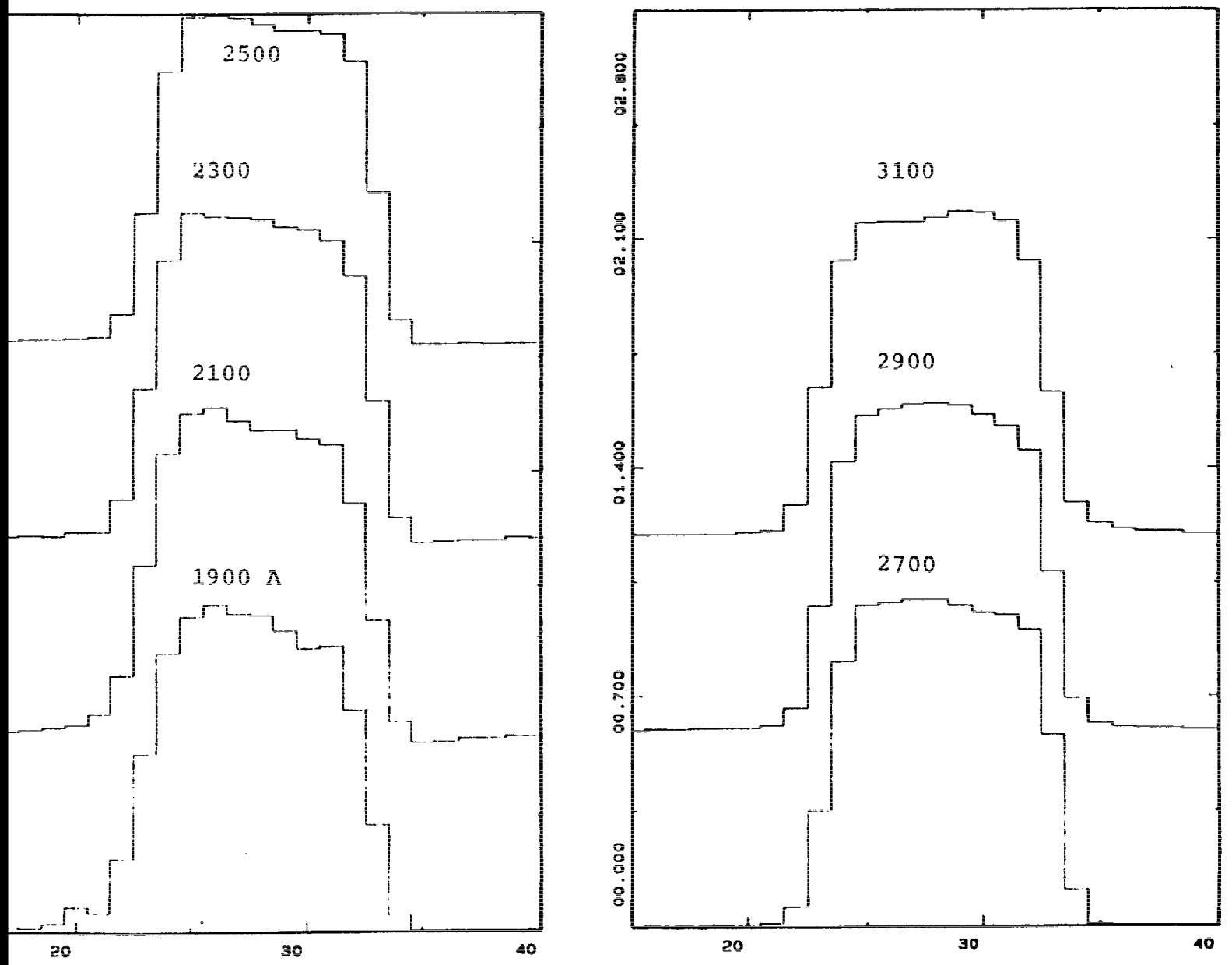
2500
2300
2100
1900 A
20
30
40
02.800
02.100
01.400
00.700
00.000
3100
2900
2700
20
30
40

- FIGURE 12b -

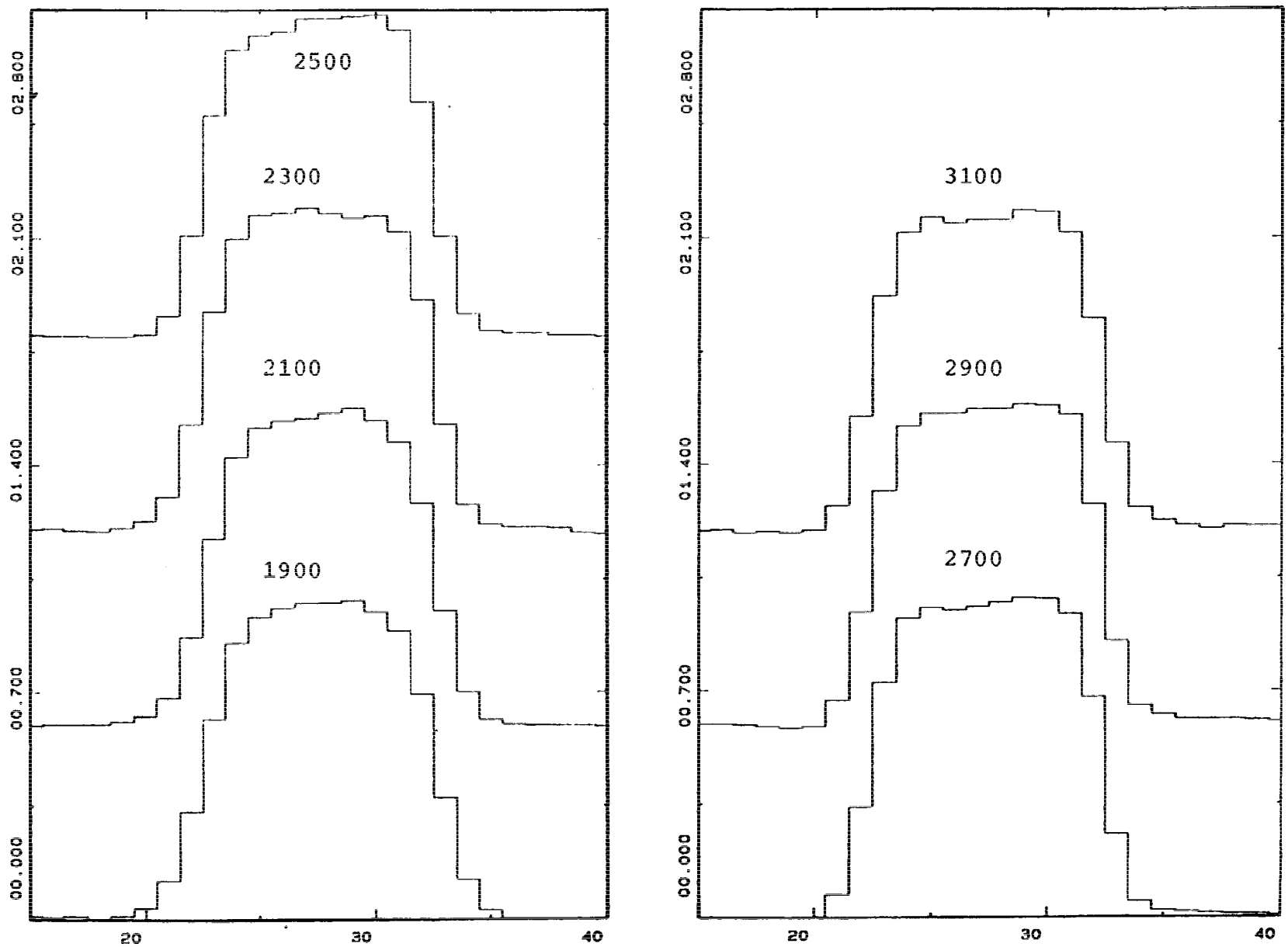
2500
2300
2100
1900
3100
2900
2700
02.800
02.100
01.400
00.700
00.000
20
30
40

- FIGURE 12c -

REFERENCES

Boggess, A. et al., 1978, Nature 275, 377

Barbero, J., Cassatella, A., 1982, Report 3 Agency Meeting VILSPA, September 1982.

Barbero, J., Cassatella, A., 1983, Report 3 Agency Meeting London, March 1983.

Cassatella, A., Penston, M.A.J., 1978, internal memorandum

Clavel, J., 1980, Report 3 Agency Meeting, GSFC

de Boer, K.S., Koornneef, J., Meade, M.R., 1980, NASA CP-2171, p. 771.

Fricke, K.H., 1983, preprint

Imhoff, C., 1983, Report presented at the User's Meeting, GSFC, March 1983.

Panek, R.J., 1982, Report 3 Agency Meeting, VILSPA

Panek, R.J., 1983, NASA IUE Newsletter, No 20 p. 52.

Ponz, D., Cassatella, A., 1981, Report 3 Agency Meeting, GSFC.